International Journal of Thermophysics, Vol. 16, No. 4, 1995

Optical Measurements of Thermal Diffusivity of a Material

H. K. Park,[1] C. P. Grigoropoulos,[1] and A. C. Tam[2,3]

Received October 14, 1994

The measurement of thermal diffusivity of a material (in particular, a thin film) is important for various reasons, e.g., to predict the heat transfer in the solid subjected to a thermal process, to monitor surface composition or morphology, or to detect invisible subsurface defects like delaminations. This measurement can be done in a noncontact manner using various photothermal methods. Such methods typically involve pulsed heating of the surface by small amounts using a laser source; the decay of the surface temperature after this pulsed photothermal heating is then probed to provide the thermal diffusivity. Various probing methods have been developed in the literature, including the probing of reflection, refraction, and diffraction from the pulsed heated area, infrared thermal radiometry, and surface deformation. This paper provides an overview of such techniques and some examples of their applications.

KEY WORDS: heat transfer; optical diagnostics; photothermal methods; thermal diffusivity.

1. INTRODUCTION

The thermal diffusivity D of a material is an important thermal property that determines the rate of transient heating and cooling processes. The thermal diffusivity D is related to the thermal conductivity K, density ρ, and specific heat C by the relationship

$$D = \frac{K}{\rho C} \tag{1}$$

[1] Department of Mechanical Engineering, University of California, Berkeley, California 94720, U.S.A.

[2] IBM Almaden Research Center, 650 Harry Road, San Jose, California 95120-6099, U.S.A.

[3] To whom correspondence should be addressed.

0195-928X/95/0700-0973$07.50/0 © 1995 Plenum Publishing Corporation

Traditional methods to measure D for solids usually rely on "contact measurements," whereby temperature sensors are attached onto the solid surface to measure the temperature variations induced by a transient heating source [1]. Noncontact techniques are frequently more desirable, especially for a solid sample that is small in size or in thickness. Such techniques are possible using a noncontact heating source (e.g., a pulsed laser beam) and a noncontact temperature measurement technique (e.g., monitoring thermal radiation, surface reflectivity, refractive-index changes, etc.). This paper provides a review of some of these noncontact techniques that can be used to measure thermal diffusivities, as well as some examples of recent experiments.

2. GENERAL DESCRIPTION OF OPTICAL MEASUREMENT OF THERMAL DIFFUSIVITY

The technique of optical measurement of thermal diffusivity generally involves a transient heating scheme for a sample and an optical probe to detect the thermal diffusion in the sample. If the sample is opaque to the excitation radiation, the case of surface heating is achieved (which is usually the case of choice), while if the sample is weakly absorbing to the excitation, bulk heating is obtained.

The pulsed or modulated excitation source is used to induce an initial temperature profile in the material. Several kinds of initial temperature profiles have been utilized, for example (Fig. 1),

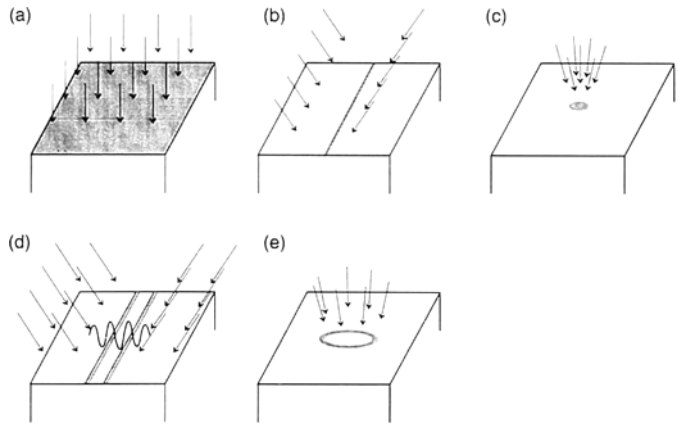

Fig. 1. Shapes of photothermal excitations useful for thermal diffusivity measurements: (a) large-area surface heating, (b) line heating, (c) small spot heating, (d) grating heating, and (e) circular heating.

(1) large-area surface heating,

(2) line heating,

(3) small spot heating,

(4) grating heating, and

(5) circular heating.

Except for the first case of heating a large area of a surface, all other cases of heating involve thermal diffusivity in more than one direction, and hence would be sensitive to any anisotropy of the thermal diffusivity. The boundary condition imposed by the sample shape also plays a role; for example, if an opaque sample in the form of a plate is excited on one side, the thermal diffusion is "slowed down" by the presence of the back surface after a characteristic time related to the thickness and the thermal diffusivity of the plate.

The optical probing of the thermal diffusion can be performed either at the vicinity of the surface of the sample (preferred) or inside the sample. Such optical probes include

(1) observation of the transient thermal radiation from the surface,

(2) refraction of the probe beam due to a thermal refractive index gradient,

(3) reflection of the probe beam at the surface with a temperature-dependent surface reflectivity,

(4) diffraction of the probe beam due to a thermally induced grating, and

(5) detection of the surface deformation.

The temporal decay of each of these parameters for the case of a pulsed excitation source (or the phase-angle change of these parameters for the case of a continuously-modulated excitation source) is related to the thermal diffusivity of the sample. Figure 2 illustrates the schematic of optical probe methods. This paper is aimed at providing some typical examples for possible combinations of the excitation and detection schemes and recent related developments, without intending to be complete or exhaustive. We review the first three kinds of optical probes in the following sections. The fourth kind, transient thermal grating (TTG) techniques, has been examined recently elsewhere [2–4]. The fifth method is based on the detection of the thermal expansion of a surface upon absorption of optical excitation [5]. Vintsents and Sandomirskii [6] applied this technique to

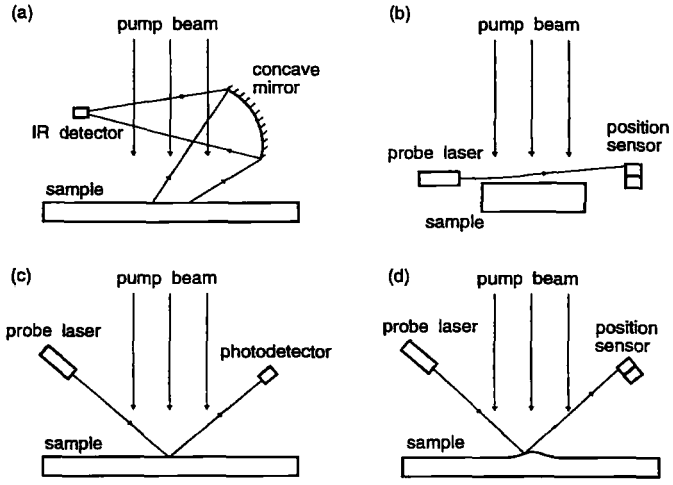

Fig. 2. Schematic of optical detection methods for thermal diffusivity measurements: (a) transient thermal radiation from the surface, (b) refraction of the probe beam due to a thermal refractive index gradient, (c) thermoreflectance at the surface, and (d) surface deformation.

measure the thermal diffusivity of metallic films. The theoretical treatment of pulsed photothermal deformation is given by Li [7]. Table I summarizes possible combinations of excitation and detection schemes.

The other kind of optical probe utilizes photoacoustic phenomena, i.e., it detects acoustic wave rather than thermal wave. This method is indirect and "inverse," requiring accurate knowledge of the photothermoacoustic energy conversion. Comprehensive reviews of optical detection of photoacoustic wave appear elsewhere [8–12].

Table I. Summary of Optical Measurement Techniques of Thermal Diffusivity. The Symbol * Indicates the Technique is Generally Adopted or Used, and the Symbol ** Indicates the Technique is Popularly Used. Typical Examples in Literature are Cited.

	Excitation method				
Detection method	Large area	Line	Small spot	Grating	Circular
Thermal radiation	**[28, 34]	*	*		*
Probe beam refraction	*	*[45]	**[13, 22]	*	
Surface reflectivity	**[59]	*	*	*	
Probe beam diffraction				*[3]	
Surface deformation		*	**[6]	*[2]	

3. THERMAL DIFFUSION FOR TYPICAL PULSED HEATING CONDITIONS

The time-dependent temperature profiles for several typical short-pulsed heating conditions are described below; this includes large area heating of a semiinfinite opaque material or of a finite slab, and small spot heating of a semiinfinite opaque material.

Figure 3 shows the schematic of the system studied. Either a semi-infinite or a finite solid material is in contact with surrounding "coupling" fluid. The solid is so-called "thermally thick" when the thermal diffusion length μ_t is smaller than the characteristic dimension l of the solid material i.e., $\mu_t \ll l$, while it is so-called "thermally thin" when $\mu_t \gg l$. The thermal diffusion length is equal to $\sqrt{\gamma D \tau_p}$, where γ is a certain constant and τ_p is the pulse width for the pulsed laser heating or the period of excitation for the continuously-modulated heating case. The characteristic dimension of the material can be the sample thickness, the distance between pump position and probe position, or the grating fringe spacing. The constant γ depends on the geometry of the sample and the configurations of the excitation source as discussed in the following section. In addition, the material is classified as "optically thick" if the optical penetration depth μ_a is smaller than l, $\mu_a \ll l$, while it is "optically thin" if $\mu_a \gg l$. It is noted that a material can be optically thick to a pump beam but optically thin to a probe beam, and vice versa. It is desirable for a material to be optically thick to the pump beam, in which case a steep thermal gradient is formed inside the material. Previous workers introduced deliberately an opaque coating layer such as carbon spray or evaporated gold film on an optically thin material [13]. We explore only the optically thick (to a pump beam) cases but discuss a few cases in the optically thin limit later.

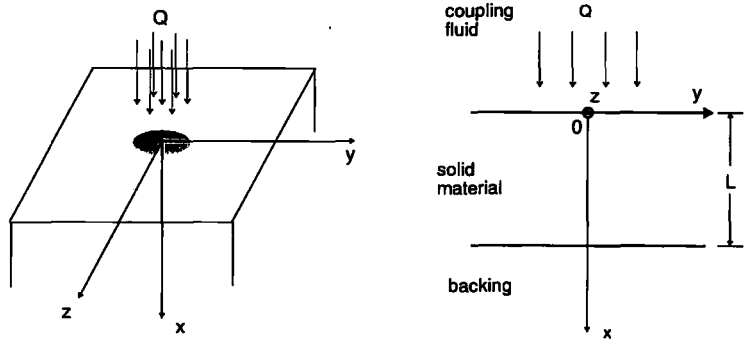

Fig. 3. Schematic geometry of sample.

In the typical cases of optical measurements, the surrounding fluid stays motionless. Therefore, convective heat transfer and viscous dissipation due to bulk motion of fluid are negligible. It is also assumed that radiation heat losses can be neglected. The heat diffusion equation is then written as

$$\rho C \frac{\partial T}{\partial t} = \nabla(K \nabla T) + Q_{ab}(\vec{x}, t) \tag{2}$$

In the above equation, $Q_{ab}(\vec{x}, t)$ is the pump beam energy absorption in the material per unit volume. The simplest behavior of monochromatic light absorption is an exponential decay (Beer's law or Bouguer's law):

$$Q_{ab}(\vec{x}, t) = (1 - \mathscr{R})\, I(t)\, \alpha e^{-\alpha x} \tag{3}$$

where $\mathscr{R}$ is the reflectivity of a material at the pump beam wavelength, α is the linear absorption coefficient, and $I(t)$ is the incident pump beam intensity.

To provide a physical insight, the following simplifications are made.

(1) The surrounding fluid is transparent to the pump beam.

(2) The material is homogeneous and isotropic.

(3) The material properties are not dependent on temperature.

(4) The pump-beam optical penetration depth is infinitesimal (i.e., skin absorption).

(5) The pump beam is of infinitesimal duration occurring at $t = 0$ (i.e., flash heating).

Absorbing fluids are not usually employed. However, absorbing fluids or transparent fluids "doped" with absorbing particles or solutes are used when the fluid is under study rather than the solid [14, 15].

Inhomogeneous or anisotropic materials are often of interest. Recently Korpiun and Osiander [16] studied powdered and microporous materials. Rantala et al. [13, 17] presented in their recent papers a method to determine anisotropic material thermal diffusivities in two different directions using two orthogonal probe beams. The possibility of detecting inhomogeneities inside materials by optical techniques has drawn enormous attention in nondestructive materials evaluation (NDE). For example, Ma et al. [18] have investigated the depth profile in laser-processed steels by probing the thermal diffusivity of the sample. A comprehensive review of photothermal NDE by thermal diffusivity measurement is given by Busse and Walther [19].

When the excitation intensity is moderate, the temperature change induced in the material is small. Under this condition, the material properties are assumed to be "constant." However, it is fair to state that the measured thermal diffusivity is "averaged" over the induced temperature range.

The skin absorption approximation is valid in most cases because opaque materials have a very shallow optical penetration depth ($\ll 1\ \mu$m) in the ultraviolet to visible wavelength range. Leung and Tam [20] analyzed the case of finite absorption depth. Heat transfer modeling of laser interactions with semitransparent solids has been studied by Grigoropoulos et al. [21]. Thermal diffusivity measurements in optically thin materials have been investigated by Salazar et al. [22, 23].

Continuous-modulated excitation or step excitation has been examined [23, 24]. Leung and Tam [20] considered the effect of finite pulse width for a pulsed excitation. In general, the effect of the excitation pulse width can be ignored if the pulse width τ_p is much shorter than the characteristic thermal diffusion time constant τ_d given by

$$\tau_d = \frac{l^2}{\gamma D} \tag{4}$$

where γ is a certain numerical constant. This instantaneous heating approximation together with the skin absorption approximation render the solution to Eq. (2) very simple, frequently in closed form expressions, via the Green's function method. In addition, the thermal coupling between the surrounding fluid and the target solid material becomes mathematically linear.

Under these simplifications, the heat conduction equation is written as

$$\frac{\partial T_i}{\partial t} = D_i \nabla^2 T_i \tag{5}$$

where the subscript i is f (coupling fluid), s (solid material), or b (backing), subject to the boundary conditions

$$T_i = 0 \qquad \text{at} \quad x = \pm\infty \tag{6}$$

$$T_f = T_s \qquad \text{at} \quad x = 0 \tag{7}$$

$$q(t) = K_f \frac{\partial T_f}{\partial x} - K_s \frac{\partial T_s}{\partial x} \qquad \text{at} \quad x = 0 \tag{8}$$

$$T_s = T_b \qquad \text{at} \quad x = L \tag{9}$$

$$K_s \frac{\partial T_s}{\partial x} = K_b \frac{\partial T_b}{\partial x} \qquad \text{at} \quad x = L \tag{10}$$

and initial conditions

$$T_i = 0 \qquad \text{at} \quad t = 0 \tag{11}$$

In Eq. (8), $q(t)$ is the absorbed heat flux and can be represented by the delta function δ as

$$q(t) = q\delta(t) \tag{12}$$

We provide a few typical examples of the temporal temperature distributions and their physical implications to the thermal diffusivity measurement. Other examples such as continuously-modulated Gaussian beam heating can be found elsewhere [23, 25].

3.1. Large Area Surface Heating

3.1.1. Semiinfinite Materials

The case of a junction of two semiinfinite materials under an instantaneous unit plane source at the interface $x = 0$ at $t = 0$ is treated by Carslaw and Jaeger [26]. The temperature distributions in the coupling fluid and the solid material are

$$T_f = \frac{K_f \sqrt{D_s}}{K_f \sqrt{D_f D_s} + K_s D_f \sqrt{\pi t}} \frac{1}{\sqrt{\pi t}} e^{-x^2/4D_f t} \tag{13}$$

$$T_s = \frac{K_f \sqrt{D_s}}{K_f \sqrt{D_f D_s} + K_s D_f \sqrt{\pi t}} \frac{1}{\sqrt{\pi t}} e^{-x^2/4D_s t} \tag{14}$$

For a heat source of strength Q, using the energy conservation for the overall system, i.e.,

$$\int_{-\infty}^{0} \rho_f C_f T_f \, dx + \int_{0}^{\infty} \rho_s C_s T_s \, dx = Q \tag{15}$$

the temperature in the fluid and the solid material can be therefore written as

$$T_f = \frac{Q}{\rho_f C_f \sqrt{D_f} + \rho_s C_s \sqrt{D_s}} \frac{1}{\sqrt{\pi t}} e^{-x^2/4D_f t} \tag{16}$$

$$T_s = \frac{Q}{\rho_f C_f \sqrt{D_f} + \rho_s C_s \sqrt{D_s}} \frac{1}{\sqrt{\pi t}} e^{-x^2/4D_s t} \tag{17}$$

It is noted that the temperature distribution has the form given by the superposition of two separate solutions of semiinfinite materials under instantaneous heat sources of intensities:

$$Q_f = \frac{Q\rho_f C_f \sqrt{D_f}}{\rho_f C_f \sqrt{D_f} + \rho_s C_s \sqrt{D_s}} \tag{18}$$

$$Q_s = \frac{Q\rho_s C_s \sqrt{D_s}}{\rho_f C_f \sqrt{D_f} + \rho_s C_s \sqrt{D_s}} \tag{19}$$

where Q_f represents the amount of heat diffused into the fluid and Q_s represents the amount of heat diffused into the solid. It can be easily confirmed that $Q_f + Q_s = Q$. The ratio of Q_f and Q_s is determined by $\sqrt{\rho_f C_f K_f}/\sqrt{\rho_s C_s K_s}$. As an example, for a bulk nickel in air, Q_f/Q_s is calculated to be 0.0003 (0.03%) [27].

An optical measurement of thermal diffusivity is based on the observation of the evolution of the temperature profile. If this is to be done for an opaque solid material, a probe beam can monitor only the solid surface or the coupling fluid. The temperature profile in the coupling fluid also contains information on the thermal properties of the solid material [Eq. (16)], so it is possible to extract solid material properties by probing the coupling fluid.

To describe thermal diffusivity measurements, we examine the temporal evolution of the temperature at a certain location away from the surface, i.e., $|x| > 0$. At early times, i.e., $t < x^2/4D$, the exponential term in Eqs. (16) and (17) is nearly zero; the right-hand sides of Eqs. (16) and (17) vanish and the temperature rises slowly with time. When the time is comparable to the characteristic thermal diffusion time, $\tau_d = x^2/4D$, the temperature reaches a maximum. At later times, i.e., $t \gg \tau_d$, the exponential term is nearly 1 and the inverse square root term becomes dominant; the temperature decays following the inverse square root of time. Hence, there exist three ways to measure the thermal diffusivity from the temperature evolution information: first, on the basis of the temperature rise rate; second, from the temporal occurrence of temperature maxima; and finally, from the analysis of temperature decay. Of these three, the monitoring of the temperature maxima is easier and more well defined. The time at which the temperature is maximum at a point x is obtained by $\partial T_i(x)/\partial t = 0$, where the index i denotes either a solid or a fluid. Therefore, the temporal position of the temperature maxima t_{max} is calculated to be twice the characteristic thermal diffusion time as

$$t_{max} = 2 \times \tau_d = \frac{x^2}{2D_i} \tag{20}$$

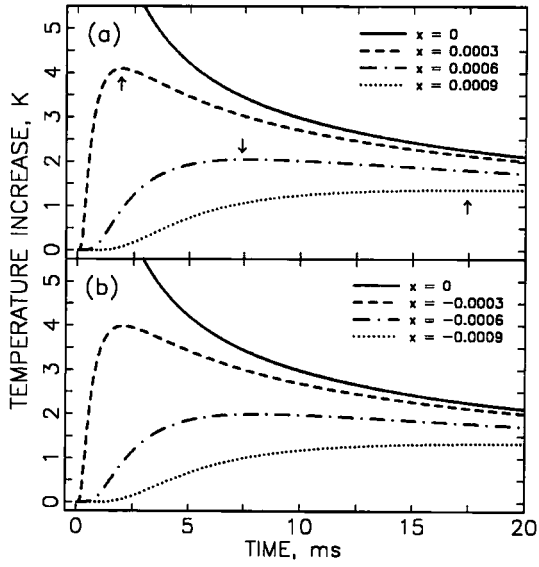

Fig. 4. Temperature histories at various locations inside (a) semiinfinite nickel and (b) air after the release of a planar heat source of intensity 1 J cm^{-2} at the interface $x=0$ at $t=0$. Values of x are in m.

Therefore, the thermal diffusivity can be easily converted from the measured value of t_{max}. Multipoint regression analysis would enhance the accuracy of measurements. For most of substances t_{max} is observable by optical methods. When this is not possible, monitoring of a temperature decay rate is an alternative. Figure 4a shows the temperature evolution at several locations inside nickel after a release of heat of intensity 1 J cm^{-2} at $t=0$ (note that 1 J cm^{-2} is not the incident fluence but the "absorbed" energy density). The arrows in Fig. 4a indicate t_{max} for the corresponding positions, x. Figure 4b shows the temperature evolution at several locations in air side, indicating that the temperature profile is almost "symmetric." This is because the thermal diffusivity of air (2.18×10^{-5} m^2 s^{-1}) is close to that of nickel (2.31×10^{-5} m^2 s^{-1}). Therefore, heat diffuses into air as fast as into nickel. This fact provides a basis for the probe beam refraction technique.

3.1.2. Finite Slab

Carslaw and Jaeger [26] also gave solutions for the transient temperature field in the composite structure of a finite slab of thickness l and a semiinfinite material. When the temperature at $x=l$ is fixed at 0, the

temperature profile in the slab upon application of a unit heat source at $x=0$ is given as

$$T_s=\frac{\sigma}{(1+\sigma)\sqrt{\pi D_f t}}\sum_{n=1}^{\infty}\alpha^n\left\{\exp\left[-\frac{(x-2nl)^2}{4D_s t}\right]-\exp\left[-\frac{\{x+2(n+1)\,l\}^2}{4D_s t}\right]\right\} \tag{21}$$

where

$$\alpha=\frac{\sigma-1}{\sigma+1},\qquad \sigma=\frac{K_f}{K_s}\sqrt{\frac{D_s}{D_f}} \tag{22}$$

while the temperature profile in the surrounding fluid remains essentially the same as given in Eq. (13). For a heat source Q, the temperature is a constant multiple of Eq. (21), where the constant is obtained by the energy conservation relation, Eq. (15).

3.2. Small Spot Heating

The small spot heating is a general term for a three-dimensional heating scheme. In many cases of thermal diffusivity measurement, small spot heating scheme is utilized because of its ability to resolve anisotropic properties. The heating can have any spatial intensity shape (disk, square, ellipse, or arbitrary). The mathematical solution of this type usually involves double and/or triple integrals, using arrays of sources and/or sinks [26]. Numerical solutions are often desirable due to the complexity of analytical solutions. Since we aimed at providing physical insights rather than addressing mathematical complexity, we examine the simplest limiting case, namely, a point source. In general, the point source approximation is valid if the pump beam spatial dimension, for example, the laser beam radius, is much smaller than the characteristic lateral dimension, for example, the lateral probe beam offset.

3.2.1. Semiinfinite Materials

The analytical solution is given by Carslaw and Jaeger [26] for an infinite composite material when a unit instantaneous heat source is released at the origin.

$$T_s=\frac{k^2}{8\pi^2(D_f t)^{3/2}}\int_0^1\frac{\exp[-k^2R^2/4(k^2u+1-u)]}{(k^2u+1-u)\,u^{1/2}(1-u)^{1/2}}f(Z,k,\sigma,u)\,du \tag{23}$$

where

$$f(Z,k,\sigma,u)=\frac{kZ(1-u)}{(1-u+\sigma^2u)^2}\exp\left\{-\frac{k^2Z^2}{4(1-u)}\right\}$$
$$+\sigma\sqrt{\frac{\pi u(1-u)}{(1-u+\sigma^2u)^3}}\left\{1-\frac{k^2Z^2}{2(1-u+\sigma^2u)}\right\}$$
$$\times\operatorname{erfc}\left\{\frac{\sigma kZ}{2}\sqrt{\frac{u}{(1-u)(1-u+\sigma^2u)}}\right\}$$
$$\times\exp\left\{-\frac{k^2Z^2}{4(1-u+\sigma^2u)}\right\} \tag{24}$$

$$Z=\frac{x}{\sqrt{D_f t}},\qquad R=\sqrt{\frac{x^2+y^2+z^2}{D_f t}},\qquad \sigma=\frac{K_s}{K_f}\sqrt{\frac{D_f}{D_s}},\qquad k=\sqrt{\frac{D_f}{D_s}} \tag{25}$$

An expression for T_f can be found in the same way by interchanging the subscripts f and s.

Figure 5 shows the calculated temperature evolution at various locations on the surface of nickel in air after an instantaneous release of heat of energy 1.0 J at the origin. Phase change is not assumed. Compared with the one-dimensional case (Fig. 4), the heat decay is faster in later times. The heat decay is governed by $t^{-n/2}$, where n is the number of dimensions. The arrows indicate t_{max} positions in Fig. 5. The calculation of t_{max} can be made by setting the time derivative of T equal to zero, $\partial T/\partial t=0$ as

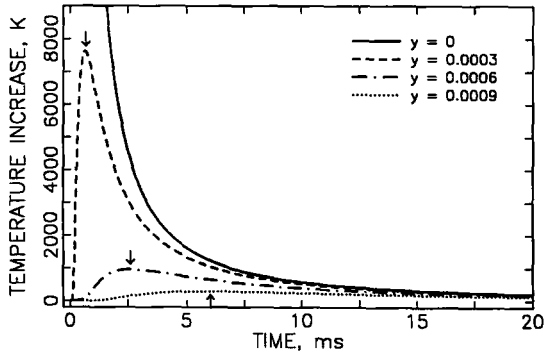

Fig. 5. Temperature histories at various locations on the surface of a semiinfinite nickel slab in air after a release of point heat source of intensity 1 J at the origin at $t=0$. Values of y are in m.

Table II. Characteristic Length Scales l and Characteristic Thermal Diffusion Time Constants τ_d for Typical Heating Cases [2, 20]

Heating case	l	τ_d
1-D semiinfinite	Distance from heat source x	$x^2/4D$
1-D finite slab	Slab thickness L	$L^2/\pi^2 D$
3-D semiinfinite	Distance from heat source r	$r^2/12D$
1-D grating	Grating fringe spacing Λ	$\Lambda^2/4\pi^2 D$

demonstrated in Section 3.1.1. When k is 1, i.e., thermal diffusivities of coupling fluid and solid material are equal, t_{max} can be easily derived by a simple relation as

$$t_{max} = \frac{x^2 + y^2 + z^2}{6D_s} \tag{26}$$

Therefore, t_{max} for three-dimensional heating is one-third of that for one-dimensional heating. Figure 5 shows that $t_{max;\,3\text{-}D}$ is exactly one-third of the $t_{max;\,1\text{-}D}$ depicted in Fig. 4 (recall that the thermal diffusivity of air is almost the same as that of nickel).

We have so far discussed the importance of the characteristic thermal diffusion time constant on the thermal diffusivity measurement. We have also demonstrated that the thermal diffusivity can be directly converted by measuring a certain characteristic time constant. Table II summarizes the characteristic thermal diffusion time constant of typical cases.

4. EXAMPLES OF OPTICAL DETECTION TECHNIQUES

4.1. Pulsed Photothermal Radiometry

The technique of pulsed photothermal radiometry (PTR) relies on the observation of the rate of cooling of the surface after pulsed laser heating by monitoring the transient thermal emission from the surface. The cooling rate of the surface can be analyzed to provide a value of the thermal diffusivity of the solid. Consider the case of a solid plate of thickness L that is opaque to the irradiation wavelength λ_1 and to the observation wavelength λ_2. A simplified one-dimensional analysis can be used for "large area irradiation," when the irradiation area is much larger than L. The detected transient infrared (IR) signal $S(t)$ is

$$S(t) = G\varepsilon\sigma_{SB}(T(t)^4 - T_0^4) \tag{27}$$

where G is a constant depending on the electronic gain and the detector spectral bandwidth, ε is the emissivity of the sample surface averaged over the detector bandwidth, σ_{SB} is the Stefan–Boltzmann constant, and T_0 is the ambient temperature. The theoretical analysis for the PTR of a one-dimensional plate is given by Leung and Tam [20].

In a typical PTR measurement, the observation spot can, in principle, be anywhere on the sample; however, the infrared emission is usually detected at the excitation spot in a backward direction ("back-detected" or "single-ended" PTR) or from a spot that is "end-on" through the sample thickness from the excitation spot ("transmission" or "double-ended" PTR) [9]. Figure 2a illustrates the schematic of back-detected or single-ended PTR.

The main advantage of PTR technique is its rather general applicability; a sample can be in vacuum, in very hot or cryogenic environment, or far away from a detector. In addition, PTR is not sensitive to the "status" of a sample; it can be a liquid, a foil, or an inhomogeneous material. Inhomogeneous materials such as papers and U.S. currency notes [28] and epoxy powders [29] have been studied by PTR. One of the disadvantages of PTR is its low temporal resolution compared to other optical probes. Usually IR detectors are not as fast as visible light photodetectors which have a pico- to nanosecond rise time. Difficulty arises when the thermal diffusivity of thin film is to be measured. Consider a 1-μm-thick nickel film. The characteristic thermal diffusion time constant is $\tau_d = (L^2/4D) \sim 10$ ns. Hence, heat spreads out across the film in a few tens of nanoseconds. To measure the thermal diffusivity of such a film, a detector

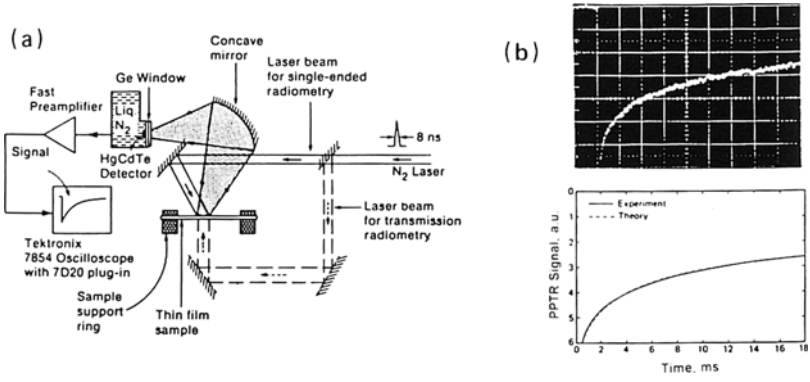

Fig. 6. Example of pulsed photothermal radiometry (PTR) [28]: (a) experimental arrangement and (b) observed back-detected PTR signal for a Teflon film of thickness 89 μm after a nitrogen laser pulse ($\tau_p = 8$-ns FWHM and $\lambda = 337$ nm) shown together with fitting of the signal by theory [20, 28]. The horizontal scale in the observed signal is 2 ms per division.

must have a nanosecond time resolution and PTR becomes less competitive compared to other optical techniques. Perspectives of PTR and reviews of its applications have been presented by Tam [30] and Kanstad and Nordal [31, 32].

The PTR technique has been utilized to measure thermal diffusivities of numerous materials, including molten salts [33], Teflon films [28], and diamond films [34]. Figure 6 shows the observed single-ended PTR signals for a Teflon film of thickness 89 μm as well as the fitting of the signal by one-dimensional analysis given by Leung and Tam [20, 28]. The observed signal shows a sharp drop at early times, slow recovery at intermediate times, and flattening at later times after the heat is uniformly distributed across the thickness. Recently, Chen and Mandelis [34] investigated extensively the PTR measurement of diamond films, enhancing the signal-to-noise ratio significantly by rate-window spectrometry. Another method, using infrared images of evolving thermal patterns by an IR camera, has been applied by Welch et al. [35] to measure in-plane thermal diffusivities.

4.2. Probe Beam Refraction Methods

Photothermal heating of a sample can produce a refractive-index gradient (RIG) in the sample or in an adjacent "coupling fluid." There are two types of RIG produced by the photothermal heating of the sample, namely, a "thermal RIG" and an "acoustic RIG." Thermal lensing (TL) and photothermal and photoacoustic deflection detection are examples of optical techniques monitoring the thermal or acoustic RIG. We shall generally refer to these detection techniques as "probe beam refraction" (PBR) methods.

4.2.1. Classifications of PBR

Since there are many variations of PBR technique, it might be useful to classify them as follows (see Fig. 7).

- "Direct" or "internal": The probe beam is located inside the material (which is to be transparent to the probe).
  - "Collinear" or "parallel": The probe beam is in the same direction as the pump beam; the special case of this is "thermal lensing."
  - "Transverse" or "perpendicular": The probe beam is in the perpendicular direction to the pump beam.
- "Indirect" or "external": The probe beam is located outside the irradiated material (detected by the mirage effect).
  - "Skimming": The probe beam grazes the material surface.
  - "Bouncing": The probe beam is reflected on the material surface.

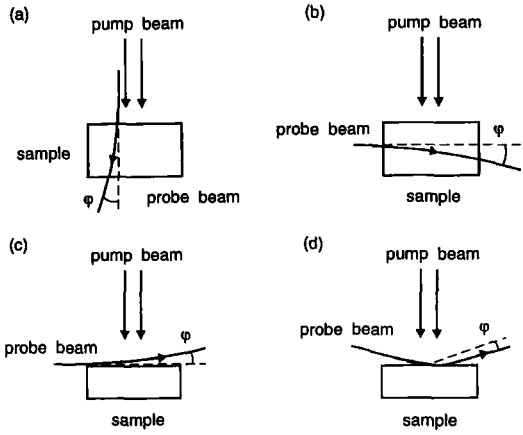

Fig. 7. Configurations of various probe beam refraction (PBR) methods: (a) direct and collinear, (b) direct and transverse, (c) indirect and skimming, and (d) indirect and bouncing. The illustrated deflection directions are for the case of $dn/dT < 0$.

The direct method can be applied when a sample is optically transparent to a probe beam; the ideal case is given when a sample is opaque to a pump beam and transparent to the probe beam. Fournier et al. [36] considered such a case, heating a silicon sample with an Ar^+ pump beam ($\lambda = 514.5$ nm) and utilizing an IR HeNe probe beam ($\lambda = 1.25$–$3.39\ \mu$m). A special case is a thin opaque film deposited on a transparent substrate. Spear and Russo [37] examined such a structure. Thermal lensing (TL) is widely used in measurements of gaseous and liquid samples [38–40]. It is noted, however, that the thermal lensing technique does not necessarily require a transparent sample. Opsal et al. [41] applied the thermal lensing technique to an opaque silicon sample. In their experiment, the probe beam incident normal to the sample surface is reflected and deflected by the thermal lens in air that is produced by the focused pump beam.

The indirect method is used for a sample that is either transparent or opaque to the probe beam. Previous theoretical studies indicate that better accuracy can be achieved by placing the probe beam closer to the surface [23, 42]. Due to the probe light diffraction and the geometrical limits of the skimming scheme, the bouncing scheme yields better results [22] if the probe beam intercepts the surface at a large angle of incidence. However, the bouncing scheme requires a sufficiently specular surface. Rough polymer materials, for instance, cannot be candidates for the bouncing scheme due to difficulty in polishing the surface. In addition, the bouncing

scheme may not be applicable to thin foil materials, where thermal expansion and bending (so-called "drum effect") complicate optical responses [22, 43, 44].

It is noted that multiple probe beam configuration may be used; Skumanich et al. [45] probed both sides of a sample film to measure thermal properties.

4.2.2. PBR in Thermal Diffusivity Measurement

Since the pioneering work by Boccara et al. [46], the mirage PBR technique has been further developed by Jackson et al. [47] and Aamodt and Murphy [42, 48, 49]. Here we examine general features of PBR due to thermal RIG and applications to thermal diffusivity measurements. Jackson et al. [47] showed that the acoustic contribution becomes significant only at very high frequencies of pump beam modulation and/or large probe beam displacements between the heat deposition region and the probe beam. In general, thermal RIG provides a larger signal compared to acoustic RIG, which, however, can have a narrower temporal profile and be detectable far away from the excitation region [9].

The PBR deflection angle is in general written as

$$\vec{\varphi}(t) = -\int \frac{1}{n}\frac{dn}{dT}\nabla T(\vec{x}, t) \times d\vec{l} \tag{28}$$

where n is the index of refraction in the medium and $d\vec{l}$ is an incremental distance along the probe beam path. Generally the PBR deflection angle has one component perpendicular and one parallel to the sample surface. The PBR angle is detected by a position sensitive optical detector such as a bicell or quadrant photodetector and a knife edge. In case of a bicell photodetector,

$$\varphi \propto \frac{V_1 - V_2}{V_1 + V_2} \tag{29}$$

where V_1 denotes the signal amplitude from cell 1 and V_2 denotes the signal amplitude from cell 2. The perpendicular and parallel components can be resolved by a quadrant detector. Aamodt and Murphy [48] showed that when measurements are made close to the sample surface, the mirage PBR angle is [50]

$$\varphi_n \propto \text{weighted mean value of } T \text{ along path} \tag{30}$$

$$\varphi_t \propto \text{weighted mean value of } \frac{\partial T}{\partial y} \text{ along path} \tag{31}$$

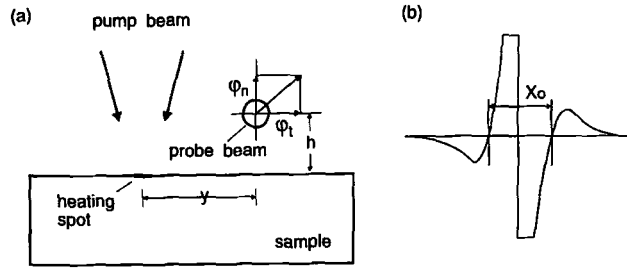

Fig. 8. Mirage probe beam refraction (PBR) experiment for thermal diffusivity measurements: (a) schematic of the experimental arrangement and (b) representative plot of the in-phase component of the transverse mirage-effect deflection, φ_t [51, 52].

where φ_n is the normal component and φ_t is the transverse component of mirage PBR deflection angle (see Fig. 8).

The application of the mirage PBR to thermal diffusivity measurement was demonstrated by Kuo et al. [51, 52]. They utilized the relation of zero-crossings of the in-phase signal of the transverse mirage-effect deflection φ_t (see Fig. 8) to the inverse root of the modulation frequency ω, i.e., $x_0 = f(1/\sqrt{\omega})$. Salazar et al. [23] later developed methods generally applicable to materials of arbitrary thickness and composition and obtained the relation

$$m = \sqrt{\Gamma D} \tag{32}$$

where m is the slope of the linear relation between the first noncentral crossings of $\mathrm{Re}(\varphi_t)$ and the inverse root of the modulation frequency $1/\sqrt{\omega}$, and Γ is a parameter that depends on the material. They also found that the value of Γ lies between 1 and 1.44.

Loulergue and Tam [15] employed "internal" and "transverse" PBR techniques to measure the thermal diffusivity of a gaseous sample. Thermal diffusivity was obtained by comparing the observed deflection signal with the following theoretical relation:

$$S(r, t) = GI'_p(r_1)\, L\varphi(r, t) \tag{33}$$

where G is a constant depending on the photodiode sensitivity and gain, $I'_p(r_1)$ is the lateral spatial derivative of the probe beam intensity distribution at the aperture position r_1, and L is the distance from the cell center to the aperture (see Fig. 9a). The observed PBR signal of a nitrogen gas doped with Freon following a CO_2 laser pulse ($\tau_p = 150\,\mu$s and $\lambda = 10.834\,\mu$m) is shown in Fig. 9b.

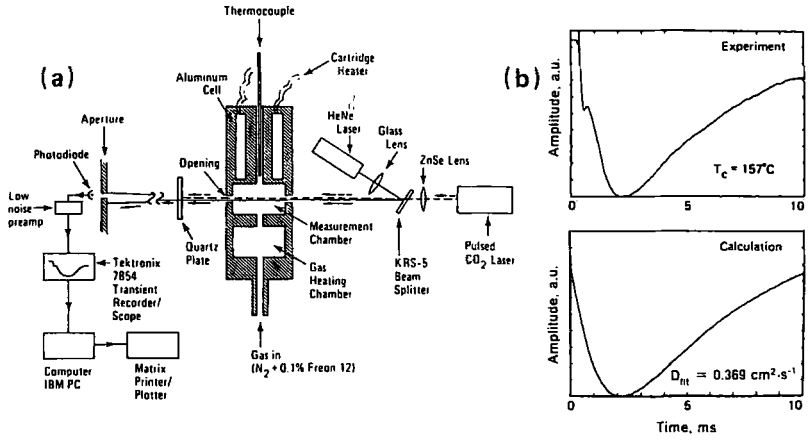

Fig. 9. Example of the probe beam refraction method [15]: (a) experimental arrangement and (b) observed photothermal deflection signal of nitrogen gas shown together with the theoretical deflection signal using the fitted value of thermal diffusivity.

The PBR technique in thermal diffusivity measurement has a merit in its versatility; it can be applied to virtually any material. However, its drawbacks sometimes cause a problem; the PBR optical alignment is more complicated compared to other optical techniques, and PBR is sensitive to vibrations, air flow currents, and other external perturbations. Previous workers used a massive solid block for an experimental setup, the so-called "mirage block" or "mirage cell," to reduce noise from environmental perturbations [13, 53]. Noise suppression in PBR has been considered by Tam [54].

4.3. Probe Reflection Monitoring

A relatively simple but reliable technique of "transient photothermal reflectance" has been used to probe temperature and/or other properties in a variety of applications. One example is encountered in processing of silicon [55, 56]. Lowndes [57] and Lompré et al. [58] have conducted optical reflectivity and transmissivity measurements on silicon samples under laser irradiation of nanosecond and picosecond durations correspondingly. Paddock and Eesley [59] later used picosecond pump and probe optical reflectivity technique to measure the thermal diffusivity of thin metal films.

This technique is based on the change of optical properties of materials with temperature. Semiconductor materials, due to enhanced temperature-dependent optical property changes, are most widely used in photothermal

reflectivity or transmission monitoring [60]. However, materials having weak variation of reflectivity upon temperature are also subject to investigations, including metals [61, 62]. Recently, Kempkens et al. [63] successfully measured the tungsten electrode temperature with the help of an integrating sphere; it is noted that the tungsten reflectivity changes by only 7% up to 2400°C.

Denoting the surface reflectivity by $\mathscr{R}$, the temperature-dependent surface reflectivity can be written as

$$\mathscr{R}(t) = \mathscr{R}_0 + \frac{d\mathscr{R}}{dT}(T(t) - T_0) \tag{34}$$

$$\frac{(\mathscr{R}(t) - \mathscr{R}_0)}{\mathscr{R}_0} = \frac{1}{\mathscr{R}_0}\frac{d\mathscr{R}}{dT}(T(t) - T_0) = C(\lambda)\frac{(T(t) - T_0)}{T_0} \tag{35}$$

where $\mathscr{R}_0$ is the surface reflectivity at initial temperature T_0. For most materials $C(\lambda)$ is of order of 10^{-5}–10^{-2} [64].

There are also other kinds of surface reflection monitoring, including piezo-reflectance probe [65] and interferometry [66]. Saenger [66] utilized an interferometric technique to capture temperature-induced optical path length changes of the reflectance from the back-side of a sample film.

One of the greatest advantages of the probe reflection technique is the ability to provide a high spatial resolution. A point-by-point mapping of

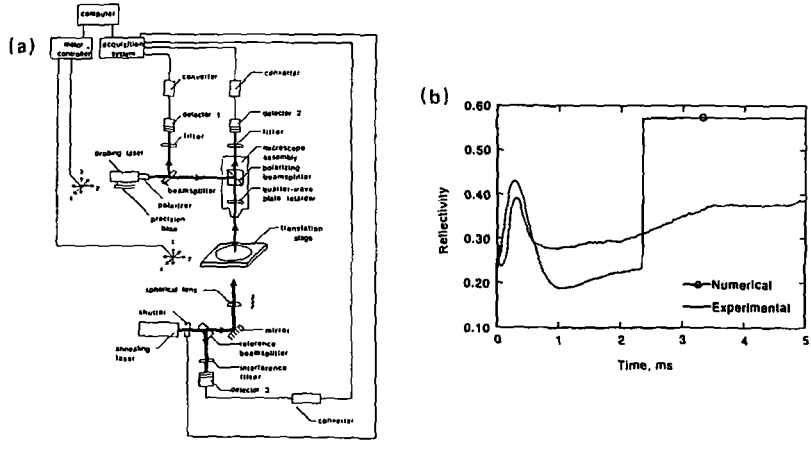

Fig. 10. Example of the photothermal reflectivity monitoring technique [67]: (a) experimental arrangement and (b) comparison between experimental and computed transient reflectivities for the 0.5-μm-thick polycrystalline silicon film on a quartz substrate heated by an argon-ion laser beam ($\lambda = 514.5$ nm, power = 1.4 W).

the surface can be achieved, as demonstrated by Guidotti and van Driel [64], who applied thermoreflectance technique to achieve defect mapping of semiconductors. It is noted that the photothermal radiometry monitors the "averaged" temperature over a finite region and the probe beam refraction detects the temperature "integrated" over a beam path. The main shortcoming of the reflection technique stems from the requirement that the surface must be optically smooth and have temperature-dependent optical properties.

An example of the reflection technique is shown in Fig. 10 [67]. It shows that the transient temperature profile in a 0.5-μm-thick polycrystalline silicon film can be captured by localized surface reflectivity measurements. In the prediction of optical reflectivity and transmissivity profiles, semitransparent films are treated as stratified multilayer structures. A characteristic transmission matrix technique is used to model the change of the refractive index due to the temperature gradient inside the sample in the calculation of the optical responses [60].

5. SUMMARY AND CONCLUSION

The thermal diffusivity of a sample can be measured optically by implanting a pulsed photothermal source on or in the sample, and by utilizing an optical probing method to detect the evolution of this photothermal profile at appropriate delay times. Such optical measurements can provide convenient, noncontact, and sensitive methods for detecting thermal properties of matter and are applicable to traditionally difficult samples in hostile environments such as in radioactive reactors or in vacuum. Furthermore, very localized or very rapid photothermal heating can be achieved to provide novel measurements or to produce new effects with a high spatial or temporal resolution, as well as to reveal subsurface and depth-dependent information.

ACKNOWLEDGMENT

Support of this work by the National Science Foundation under Grant CTS-9210333 is gratefully acknowledged.

REFERENCES

1. W. J. Parker, R. J. Jenkins, C. P. Butler, and G. L. Abbott, *J. Appl. Phys.* **32**:1679 (1961).
2. J. Jáuregui and E. Matthias, *Appl. Phys. A* **54**:35 (1992).
3. A. Harata, H. Nishimura, and T. Sawada, *Appl. Phys. Lett.* **57**:132 (1990).
4. C. D. Marshall, I. M. Fishman, R. C. Dorfman, C. B. Eom, and M. D. Fayer, *Phys. Rev. B* **45**:10009 (1992).

5. M. A. Olmstead, N. M. Amer, S. Kohn, F. Fournier, and A. C. Boccara, *Appl. Phys. A* **32**:141 (1983).
6. S. V. Vintsents and V. B. Sandomirskii, *Phys. Stat. Sol.* **133**:K7 (1992).
7. B. C. Li, *J. Appl. Phys.* **68**:482 (1990).
8. A. C. Tam, *Rev. Mod. Phys.* **58**:381 (1986).
9. A. C. Tam, in *Photothermal Investigations of Solids and Fluids*, J. A. Sell, ed. (Academic Press, London, 1988), pp. 1–34.
10. H. Sontag and A. C. Tam, *IEEE Trans. UFFC* **33**:500 (1986).
11. J.-P. Monchalin, *IEEE Trans. UFFC* **33**:485 (1986).
12. S. V. Egerev, L. M. Lyamshev, and O. V. Puchenkov, *Sov. Phys. Usp.* **33**:739 (1991).
13. J. Rantala, L. Wei, P. K. Kuo, J. Jaarinen, M. Luukkala, and R. L. Thomas, *J. Appl. Phys.* **73**:2714 (1993).
14. M. J. D. Low, C. Morterra, and J. M. Khosrofian, *IEEE Trans. UFFC* **33**:573 (1986).
15. J. C. Loulergue and A. C. Tam, *Appl. Phys. Lett.* **46**:457 (1985).
16. P. Korpiun and R. Osiander, in *Photoacoustic and Photothermal Phenomena III*, D. Bicanic, ed. (Springer-Verlag, Berlin, 1991), pp. 619–627.
17. J. Rantala, J. Jaarinen, and P. K. Kuo, *Appl. Phys. A* **55**:586 (1992).
18. T.-C. Ma, M. Munidasa, and A. Mandelis, *J. Appl. Phys.* **71**:6029 (1992).
19. G. Busse and H. G. Walther, in *Principles and Perspectives of Photothermal and Photoacoustic Phenomena*, A. Mandelis, ed. (Elsevier, New York, 1992), pp. 205–298.
20. W. P. Leung and A. C. Tam, *J. Appl. Phys.* **56**:153 (1984).
21. C. P. Grigoropoulos, H. K. Park, and X. Xu, *Int. J. Heat Mass Transf.* **36**:919 (1993).
22. A. Salazar, A. Sánchez-Lavega, and J. Fernández, *J. Appl. Phys.* **69**:1216 (1991).
23. A. Salazar, A. Sánchez-Lavega, and J. Fernández, *J. Appl. Phys.* **65**:4150 (1989).
24. H. M. James, *J. Appl. Phys.* **51**:4666 (1980).
25. R. Emmerich, S. Bauer, and B. Ploss, *Appl. Phys. A* **54**:334 (1992).
26. H. S. Carslaw and J. C. Jaeger, *Conduction of Heat in Solids*, 2nd ed. (Clarendon, Oxford, 1959).
27. R. C. Weast, *CRC Handbook of Chemistry and Physics*, 68th ed. (CRC Press, Boca Raton, FL, 1987).
28. W. P. Leung and A. C. Tam, *Opt. Lett.* **9**:93 (1984).
29. A. C. Tam and B. Sullivan, *Appl. Phys. Lett.* **43**:333 (1983).
30. A. C. Tam, *Infrared Phys.* **25**:305 (1985).
31. S. O. Kanstad and P.-E. Nordal, *Can. J. Phys.* **64**:1155 (1986).
32. P.-E. Nordal and S. O. Kanstad, *Infrared Phys.* **25**:295 (1985).
33. H. Otah, G. Ogura, Y. Waseda, and M. Suzuki, *Rev. Sci. Instrum.* **61**:2645 (1990).
34. Z. Chen and A. Mandelis, *Phys. Rev. B* **46**:13526 (1992).
35. C. S. Welch, D. M. Heath, and W. P. Winfree, *J. Appl. Phys.* **61**:895 (1987).
36. D. Fournier, C. Boccara, A. Skumanich, and N. M. Amer, *J. Appl. Phys.* **59**:787 (1986).
37. J. D. Spear and R. E. Russo, *J. Appl. Phys.* **70**:580 (1991).
38. R. Gupta, in *Photothermal Investigations of Solids and Fluids*, J. A. Sell, ed. (Academic Press, London, 1988), pp. 112–126.
39. H. Sontag and A. C. Tam, *Opt. Lett.* **10**:436 (1985).
40. J. Shen, R. D. Lowe, and R. D. Snook, *Chem. Phys.* **165**:385 (1992).
41. J. Opsal, A. Rosencwaig, and D. L. Willenborg, *Appl. Opt.* **22**:3169 (1983).
42. J. C. Murphy and L. C. Aamodt, *J. Appl. Phys.* **51**:4580 (1980).
43. K. Hane and S. Hattori, *Appl. Opt.* **29**:145 (1990).
44. G. Rousset, F. Lepoutre, and L. Bertrand, *J. Appl. Phys.* **54**:2283 (1983).
45. A. Skumanich, H. Dersch, M. Fathallah, and N. M. Amer, *Appl. Phys. A* **43**:297 (1987).
46. A. C. Boccara, D. Fournier, and J. Badoz, *Appl. Phys. Lett.* **36**:130 (1980).

47. W. B. Jackson, N. M. Amer, A. C. Boccara, and D. Fournier, *Appl. Opt.* **20**:1333 (1981).
48. L. C. Aamodt and J. C. Murphy, *J. Appl. Phys.* **52**:4903 (1981).
49. L. C. Aamodt and J. C. Murphy, *J. Appl. Phys.* **54**:581 (1983).
50. M. Munidasa and A. Mandelis, in *Principles and Perspectives of Photothermal and Photoacoustic Phenomena*, A. Mandelis, ed. (Elsevier, New York, 1992), pp. 299–367.
51. P. K. Kuo, M. J. Lin, C. B. Reyes, L. D. Favro, R. L. Thomas, D. S. Kim, S.-Y. Zhang, L. J. Inglehart, D. Fournier, A. C. Boccara, and N. Yacoubi, *Can. J. Phys.* **64**:1165 (1986).
52. P. K. Kuo, E. D. Sendler, L. D. Favro, and R. L. Thomas, *Can. J. Phys.* **64**:1168 (1986).
53. F. Charbonnier and D. Fournier, *Rev. Sci. Instrum.* **57**:1126 (1986).
54. A. C. Tam, in *Photoacoustic and Photothermal Phenomena III*, D. Bicanic, ed. (Springer-Verlag, Berlin, 1991), pp. 447–462.
55. G. E. Jellison, Jr., D. H. Lowndes, D. N. Mashburn, and R. F. Wood, *Phys. Rev. B* **34**:2407 (1986).
56. I. A. Vitkin, C. Christofides, and A. Mandelis, *J. Appl. Phys.* **67**:2822 (1990).
57. D. H. Lowndes, *Phys. Rev. Lett.* **48**:267 (1982).
58. L. A. Lompré, J. M. Liu, H. Kurz, and N. Bloembergen, *Appl. Phys. Lett.* **43**:168 (1983).
59. C. A. Paddock and G. L. Eesley, *J. Appl. Phys.* **60**:285 (1986).
60. H. K. Park, X. Xu, C. P. Grigoropoulos, N. Do, L. Klees, P. T. Leung, and A. C. Tam, *Appl. Phys. Lett.* **61**:749 (1992).
61. W. T. Walter, *Proc. SPIE* **198**:109 (1979).
62. S. D. Brorson, J. G. Fujimoto, and E. P. Ippen, *Phys. Rev. Lett.* **59**:1962 (1987).
63. H. Kempkens, W. W. Byszewski, P. D. Gregor, and W. P. Lapatovich, *J. Appl. Phys.* **67**:3618 (1990).
64. D. Guidotti and H. M. van Driel, *Appl. Phys. Lett.* **47**:1336 (1985).
65. G. Eesley, B. M. Clemens, and C. A. Paddock, *Appl. Phys. Lett.* **50**:717 (1987).
66. K. L. Saenger, *J. Appl. Phys.* **65**:1447 (1989).
67. X. Xu, S. L. Taylor, H. K. Park, and C. P. Grigoropoulos, *J. Appl. Phys.* **73**:8088 (1993).